

# The H1 Forward Track Detector at HERA II

---

**P.J. Laycock<sup>a\*</sup>, R.C.W. Henderson<sup>b</sup>, S.J. Maxfield<sup>a</sup>, J.V. Morris<sup>c</sup>, G.D. Patel<sup>a</sup> and D.P.C. Sankey<sup>c</sup>**

<sup>a</sup>*University of Liverpool,  
Liverpool L69 3BZ, UK*

<sup>b</sup>*Lancaster University,  
Lancaster LA1 4YB, UK*

<sup>c</sup>*Rutherford Appleton Laboratory,  
Didcot, Oxon., OX11 0QX, UK*

*Corresponding Author E-mail:* laycock@hep.ph.liv.ac.uk

**ABSTRACT:** In order to maintain efficient tracking in the forward region of H1 after the luminosity upgrade of the HERA machine, the H1 Forward Track Detector was also upgraded. While much of the original software and techniques used for the HERA I phase could be reused, the software for pattern recognition was completely rewritten. This, along with several other improvements in hit finding and high-level track reconstruction, are described in detail together with a summary of the performance of the detector.

**KEYWORDS:** Particle tracking detectors; Pattern recognition, cluster finding, calibration and fitting methods; Performance of High Energy Physics Detectors.

---

<sup>\*</sup>Corresponding author.

---

## Contents

<b>1. Introduction</b>	<b>2</b>
1.1 Overview of the HERA II FTD	2
<b>2. Readout and Hit Finding</b>	<b>3</b>
2.1 Introduction	3
2.2 Modifications to the algorithm	5
<b>3. H1 FTD Pattern Recognition</b>	<b>6</b>
3.1 Introduction	6
3.2 Clusters	7
3.2.1 Finding candidate clusters	7
3.2.2 Finding a final disconnected set of clusters	8
3.2.3 Cluster finding efficiency	9
3.3 Segments	9
3.3.1 Forming candidate segments	9
3.3.2 Segment forming efficiency	10
<b>4. Improvements in the Pattern Recognition using a Kalman Filter</b>	<b>11</b>
4.1 Introduction	11
4.2 Cluster addition	12
4.3 Cluster rejection	13
<b>5. Combining FTD and CTD Information</b>	<b>13</b>
5.1 Vertex fitted tracks	13
5.2 Combined FTD and CTD tracks	13
5.3 Alignment to the CTD	14
<b>6. Performance of the HERA II FTD</b>	<b>15</b>
6.1 Track selection	16
6.2 Comparisons of data and simulation for inclusive NC events	17
6.3 Comparisons of data and simulation for elastic $J/\Psi$ events	17
<b>7. Summary</b>	<b>18</b>

---

## 1. Introduction

The original HERA I incarnation of the H1 Forward Track Detector (FTD) is described in detail in [1] and much of the information found there remains relevant for the HERA II FTD. However, the luminosity upgrade of the HERA machine required a significant upgrade of the FTD in order to accommodate the higher particle multiplicities and maintain high track-finding efficiency and purity; it is these various improvements which are described here. A brief description of the upgraded FTD hardware is given in this section. Section 2 addresses the hit-finding modifications which were made in order to accommodate the higher currents in the FTD and mitigate the effects ageing in the chambers. In Section 3, a complete description of the new pattern recognition algorithms is given, while section 4 details the higher level pattern recognition modification using the Kalman Filter. Section 5 describes the combination of the FTD information together with information from the H1 Central Track Detector (CTD). Finally, Section 6 describe the performance of the FTD.

### 1.1 Overview of the HERA II FTD

A description of the H1 detector can be found elsewhere [2]. The original FTD [1] comprised various detector technologies: radial and planar drift chambers, multi-wire proportional chambers and transition radiators. The upgraded FTD reused the planar drift chambers, referred to hereafter as P-modules, and replaced all other detectors with new planar drift chambers or Q-modules. Each module has sense wires arranged parallel to one another in planes perpendicular to the  $z$ -axis<sup>1</sup> at positions between 130 and 240 cm from the nominal interaction point.

The modules were grouped into three "supermodules", as shown in figure 1. The first two supermodules contained three P-modules and two Q-modules and the third, furthest from the interaction point, had three P-modules and one Q-module<sup>2</sup>. Within a supermodule, the modules were rotated in  $\phi$  with respect to one another so that the combined drift coordinate measurements could be used to locate tracks in space. The wires in the first module were parallel to the  $y$ -axis. Subsequent modules were rotated by  $+60^\circ$ ,  $-60^\circ$ ,  $+30^\circ$  and  $+90^\circ$  with respect to this (see figure 2). In the following, the drift coordinate  $w$  is the coordinate perpendicular to the sense wires. Thus the  $w$ -axis coincides with the  $x$ -axis in the first module and is rotated with respect to the  $x$ -axis by the angles given above in the others. The three supermodules were enclosed in a gas tank through which circulated a  $Ar/C3H8$  gas mixture and which also served as a mechanical support.

The wires in each plane spanned disc-shaped regions of approximately 80 cm radius. A concentric 15 cm radius hole in the disc accommodated the beam pipe. Wires that would otherwise cross this hole were split into two separate parts. Modules contained either four wire planes (P-modules) or eight wire planes (Q-modules) separated in  $z$  by 0.6 cm. In P modules each wire plane had 32 wires spaced 5.7 cm apart across the plane. Q modules had 28 wires per wire plane, 6.2 cm apart. The drift field was maintained by a set of field wires and cathode planes surrounding the sets

---

<sup>1</sup>The origin of the H1 coordinate system is the nominal  $ep$  interaction point with the direction of the proton beam defining the positive  $z$ -axis (forward direction). The polar angle ( $\theta$ ) is defined with respect to this axis and the pseudo-rapidity is defined as  $\eta = -\ln \tan(\theta/2)$ . The azimuthal angle  $\phi$  defines the particle direction in the transverse plane.

<sup>2</sup>It should be noted that a significant fraction of the new Q-modules had significant hardware problems, with 25% of the Q-modules in the first supermodule and 50% of the only Q-module in the third supermodule being completely inoperable.

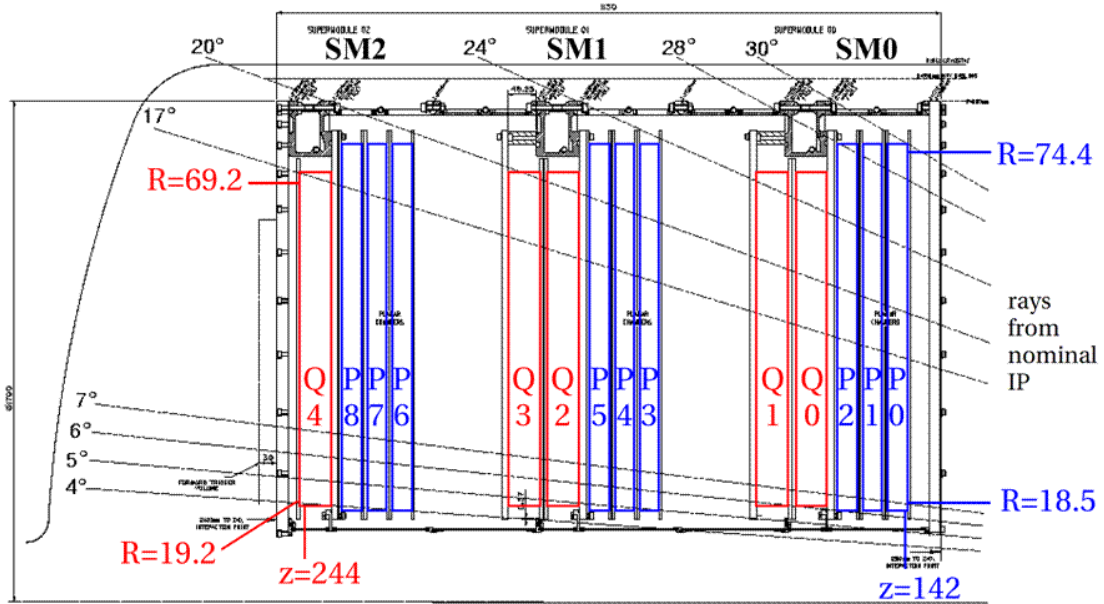


**Figure 1.** A schematic cross-section of (the top half of) the FTD showing the arrangement of modules(P, Q) within the three supermodules (SM0, SM1 and SM2). The interaction point is to the right.

of four (P-modules) or eight (Q-modules) sense wires, as shown in figure 2. Note that the wires were given a  $\pm 300\mu\text{m}$  offset ("stagger") from their nominal locations in order to help resolve "left-right" ambiguities. The wires were read out at one end only, providing a measurement of the drift coordinate perpendicular to them.

## 2. Readout and Hit Finding

### 2.1 Introduction

As with the original HERA I FTD, the sense wires in the HERA II FTD were read out using 104 MHz 8 bit non-linear Flash Analogue-to-Digital Converters (FADCs) giving a history of the chamber pulses in time-slices of 9.6 ns. The wires were instrumented at one end only. Hits, which correspond to the ionisation left behind by a charged particle passing through the detector, were found using an algorithm which analysed the charge and time information of the chamber pulses, a QT algorithm. Given the similarity between the two types of modules, the same QT algorithm was used in both to detect hits. The original version of the QT algorithm was based on that used for the old P-modules, described in [1], with the further modification of different thresholds for the "outer" wires, the wires with only one adjacent sense wire, in each set of chambers. These thresholds were implemented as an additional multiplicative factor in the relinearisation lookup table, with a nominal value of unity for the inner wires (in the Q-modules, the middle six wires) and a different factor for the outer wires. The outer wires were down-scaled by a factor of 1.9

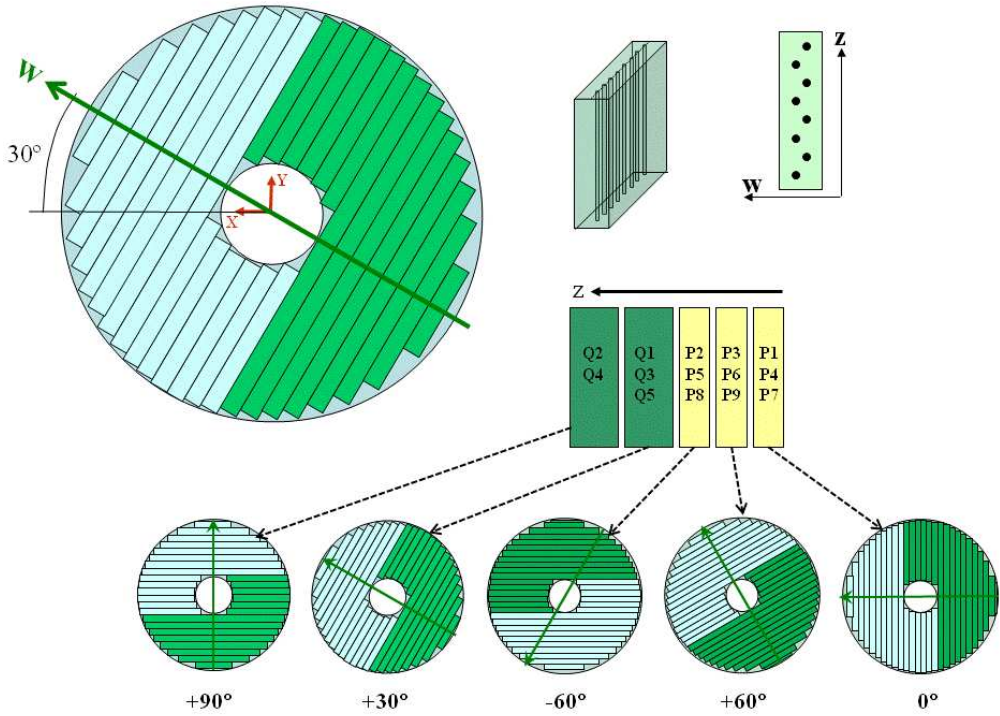


**Figure 2.** A schematic view of one supermodule of the FTD showing the orientation of wires in successive modules.

and 3.0 in the P and Q-modules, respectively, the difference arising from the different physical geometry and therefore electrostatics of the new modules.

During commissioning of the FTD with collision data, the observed single-wire efficiency of the P-modules was found to be markedly lower than expected. Extensive investigations ruled out problems with the gas mixture<sup>3</sup> or oxygen contamination<sup>4</sup> and finally revealed the first signs of ageing. Following a reanalysis of the HERA I data, it became apparent that ageing in the P-modules had already been occurring during HERA I running, but the effects of this had been masked by increases in the gain in the chambers such that the resulting inefficiencies were minimal. Upon discovering ageing, the gain (high voltage) was lowered in order to preserve the chambers. However, the result was that the P-modules became markedly inefficient at small radius. figure 3 shows mean pulse height as a function of radius for the P-modules for representative runs in 1996, 1997, 2000 and 2004 (after the reduction in gas gain) and figure 3 shows the number of hits as a function of radius for the same runs where the loss of hits at small radius is immediately apparent

<sup>3</sup>In addition to the Ar/C<sub>3</sub>H<sub>8</sub> gas mixture, ethanol was a standard component of the gas mixture at the level of  $\sim 1\%$ . Increasing the ethanol content had no effect on the gain, although the tests revealed that the operational stability of the chambers was indeed far better with the inclusion of ethanol.

<sup>4</sup>The drift time distribution was approximately flat, with known features caused by the electrostatics of the cells. There was no evidence for an inefficiency increasing with drift distance as would be expected if there was oxygen contamination. A dedicated monitor also confirmed that any possible oxygen contamination was negligible.

for the 2004 data. From the former, it is apparent that the onset of degradation was as early as 1997.

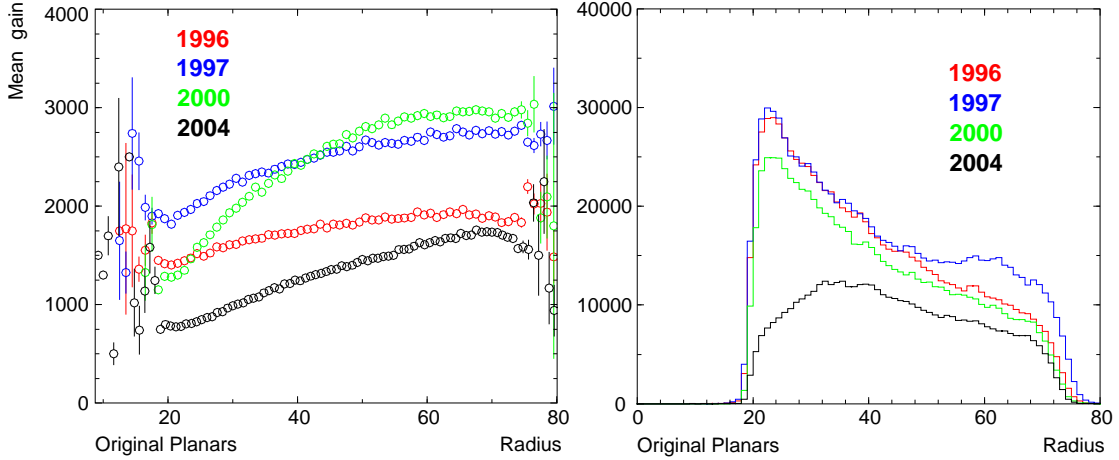


**Figure 3.** Mean pulse height as a function of radius for the P-modules for representative runs in 1996, 1997, 2000 and 2004 (left) and the number of hits as a function of radius for the same runs (right).

A new QT algorithm was then developed over the next year and implemented in 2006. This algorithm was a development of that described for the Radial chambers in [1], adapted for single-ended readout. In particular the time determination, charge determination (save for the integration interval being 8 time-slices) and overlapping hit analysis were as described previously. The major changes were in the hit detection and noise suppression, in order to enhance detection of small hits but reduce the sensitivity to noise, including the 10 MHz pickup which was an issue in some cells (in the HERA I Radial chambers this was circumvented in the hit detection by summing the signal from each end of the wire prior to the hit search).

The success of these changes can be judged from the new algorithm producing 5% fewer hits in the P-modules and 20% fewer in the Q-modules. These hits form more pattern-recognised “clusters”, which are groups of contiguous hits in a module (see section 3.2). There are 20% more hits used in P-module clusters and 5% more in the Q-modules when compared with the previous algorithm, as illustrated in figure 4 which shows the distribution of used hits as a function of radius for the P-modules nearest the interaction point in run 435774. The changes are detailed in the following.

## 2.2 Modifications to the algorithm

First, crosstalk compensation was applied using a combination of the signal and difference of samples signal ( $DOS$ , defined as  $DOS(n) = FADC(n) - FADC(n-1)$ ) of adjacent wires. Then a multistep adaptive hit search was performed, processing each wire consecutively within a block of four channels or wires (corresponding to a complete cell in the P-modules and a half-cell in the Q-modules). First, the data on the wire are scanned for potential hits consisting of a region of one or more time slices of increasing charge, corresponding to the leading edge of a potential pulse. If the total increase in charge is above a threshold then the size, location and number of such regions is recorded. At this stage, if there are no such regions in the data from a single channel, then a

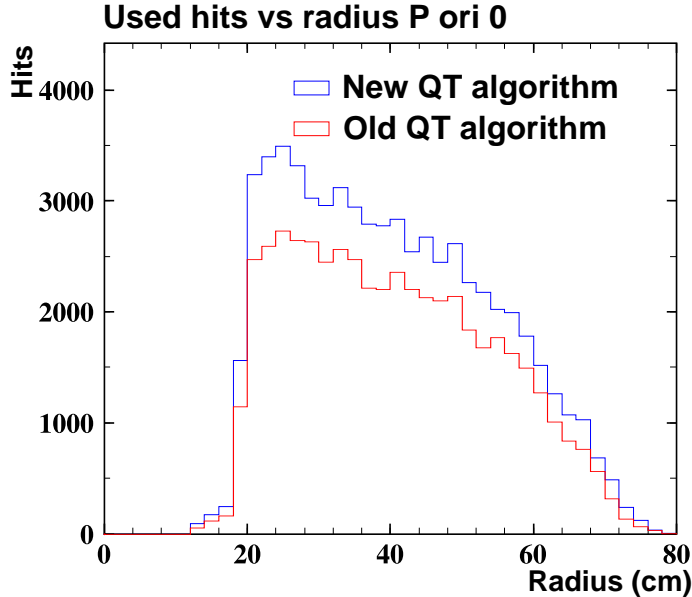


**Figure 4.** The distribution of used hits as a function of radius for the P-modules nearest the interaction point in run 435774.

single small hit is accepted if its increase in charge is greater than half the current threshold; the threshold is then modified accordingly. Next, the hit threshold is scaled up as a function of the number of potential hits found on the wire, such that the hit search is automatically hardened in the presence of multiple hits (or in particular, oscillating noise). The potential hit candidates are compared to this modified threshold (and in the case of more than one candidate, the additional requirement that there are at least two time slices on the leading edge of the pulse).

The charge is then determined for hits passing this modified threshold. If this charge is greater than twice the threshold the hit is accepted (again effecting protection against oscillating noise). Finally there is a requirement that in each block of four wires there is at least one hit above the original full threshold, failing which all hits for the wires are suppressed, as a final protection against noise. This multistep search allows a significantly lower hit threshold to cope with inefficient wires whilst maintaining robust protection against noise. For the P-modules, the hit threshold used was half that used in the original algorithm, while for the Q-modules it was  $7/8$ . The smallest hits that could be detected were therefore a quarter of the size of the minimum with the original algorithm. These changes restored the monitored single hit efficiency of the old P-modules to around 96%, matching the Q-modules, as illustrated by figure 5 taken from the on-line monitoring at the time the new algorithms went live. The successful conclusion of these changes allowed stable operation of the FTD for the remainder of the HERA II running, with an uptime of  $\sim 98\%$ .

### 3. H1 FTD Pattern Recognition

#### 3.1 Introduction

The pattern recognition for the H1 FTD is achieved in distinct stages. Firstly, the hits found by the

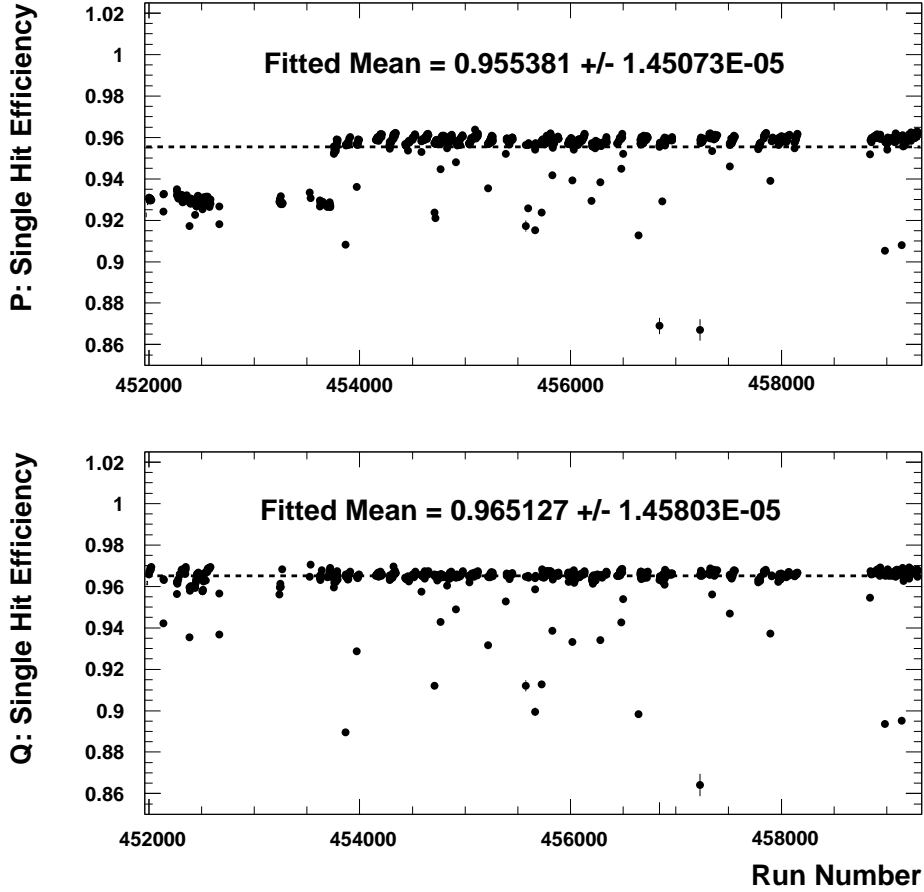


**Figure 5.** The monitored single hit efficiency of the old P-modules, the change to the new QT algorithm can be clearly seen.

QT algorithm in Section 2 are combined into clusters of hits in individual modules. These clusters are then combined at the level of supermodules to make track segments. Finally, those segments are linked together and fit using a modified version of the Kalman filter described in [1].

### 3.2 Clusters

#### 3.2.1 Finding candidate clusters

The hits identified by the QT algorithm provide sufficient information to define a plane in the drift coordinate of the module  $w$  at the  $z$  position of the module. The sign of  $w$  is ambiguous and thus there are two hit hypotheses at this stage, but thanks to the stagger in the sense wire positions the correct sign of  $w$  can be identified. If the correct sign is chosen the hits will form a straight line, whereas the "reflection" hits will be displaced by twice the sense wire stagger. This is illustrated for a single track passing through a Q-module with perfect efficiency and no extraneous pluses in figure 6.

The pattern recognition of the clusters in the original 4-wire P-modules is described in [1]. For those modules, only clusters containing a minimum of three hits were output as when there were

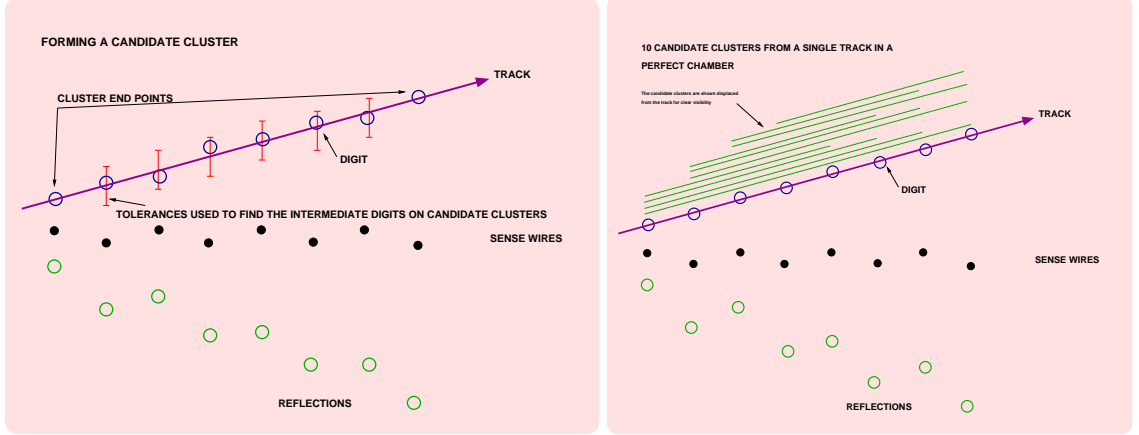


**Figure 6.** (left) Schematic of a candidate cluster in the Q chambers and (right) ten candidate clusters formed from a single track in a perfect chamber.

fewer than three hits the sign of  $w$  could not be determined<sup>5</sup>. The new 8-wire Q-modules enabled the pattern recognition to be improved as they have much higher redundancy. In these modules, except when the number of unusable wires in the module does not allow it, the minimum number of hits in a cluster is five. Studies with Monte Carlo showed that the improvements in purity and quality of clusters above five hits were less significant than below.

All the possible candidate clusters are formed using all the available information from all hits. These candidate clusters are then reduced to a disconnected set of clusters which do not have any hits in common. The candidate clusters are found by considering the straight line between any two hits in the same module which are far enough apart in  $z$  that at least three intermediate hits could be found. Any hits on the intermediate wires that are within three times the hit resolution of the hypothetical drift distance to the sense wire are accepted. If a single track is found with perfect efficiency then this algorithm will generate ten candidate clusters as shown in figure 6. This conservative approach leaves the pattern recognition robust against problems arising from e.g. two tracks in the same cell, dead or inefficient sense wires and hits originating from noise.

### 3.2.2 Finding a final disconnected set of clusters

The hits for each candidate cluster are fitted to a straight line at a fixed  $z$  which is the  $z$  value of the centre of the module. This determines the cluster position in a four-dimensional space labelled  $(X, Y, X', Y')$ , where  $X$  and  $Y$  are local analogues to the H1 coordinates and  $X'$  and  $Y'$  are the slopes in these coordinates. Each track passing through a Q-module can generate up to ten candidate clusters which form spikes in this space. The candidates in each of the four dimensions are split wherever the gap between the clusters exceeds a tuned value for that dimension. Candidate cluster spikes with fewer than three candidates are ignored. Each cluster spike is examined in turn to select the best candidate cluster that it contains.

<sup>5</sup>Indeed, the three hit cluster sample contained a significant proportion of hits with the wrong drift sign and hits from multiple tracks.

Firstly, the candidate cluster with the highest number of unique hits (hits not shared with clusters in other spikes) is considered. The straight line fit must have a probability of fit of greater than 5% and this value must be within a factor of ten of the highest probability for any cluster within the spike. If this is satisfied, this candidate is chosen and all other candidate clusters in that spike are eliminated. All remaining spikes which do not have such a candidate are considered in a second step. The same method for selecting a single cluster is used but the limit on the fit probability is reduced to 1%. If this still does not choose a candidate cluster in a spike, candidates that share clusters with other spikes are removed and the best candidate in terms of fit probability is taken.

When even a few tracks are incident on the FTD, complex situations can arise and the candidate clusters which have been chosen from the spikes can still share hits with other clusters. A very powerful technique for choosing which of these connected clusters are truly from tracks and not random combinations is to reduce these clusters to a final set of disconnected clusters. There is no unique algorithm for doing this but the method which has been found to work best for the FTD Q-modules is to remove in turn the cluster which has the highest number of connections to other clusters. If there is more than one cluster in this set then for each member of the set, a connection probability is formed from the following equation:

$$prob \left( \sum_{i=1}^n \chi_i^2, \sum_{i=1}^n v_i \right) \quad (3.1)$$

where the sum is over the set of clusters to which this cluster is connected and  $\chi$  and  $v$  are the chi-squared and number of degrees of freedom of the connected cluster. The cluster which is connected to the set of clusters with the highest connection probability is removed. After each cluster is removed, the number of connections is recalculated and the disconnection method repeated until a final, disconnected set of clusters is found.

### 3.2.3 Cluster finding efficiency

Both the cluster finding efficiency and purity need to be considered simultaneously when judging the performance of the cluster-finding algorithm. The results in table 1 show the efficiency above a given purity for 10, 20 and 30 tracks incident on the FTD. The efficiency is in general high. However, as the multiplicity increases, the track density is such that there is significant overlap of the tracks in the projections measured by the Q-modules. The requirement on purity dictates the size of the effect on the efficiency.

## 3.3 Segments

The next stage in the pattern recognition software is to identify track candidates at the level of a supermodule, referred to as segments. The clusters output from the previous stage are used as input to a segment-finding algorithm, described in the following.

### 3.3.1 Forming candidate segments

Clusters define planes which contain the trajectory of a charged particle. The modules are rotated in  $\phi$  with respect to  $\phi = 0^\circ$ , such that modules have a unique orientation within a supermodule (see

**Table 1.** Efficiency for cluster finding for a given number of tracks in the FTD. For simulation, the efficiency is given for varying minimum requirements on purity, while for data the observed efficiency is shown. The statistical uncertainties are negligible.

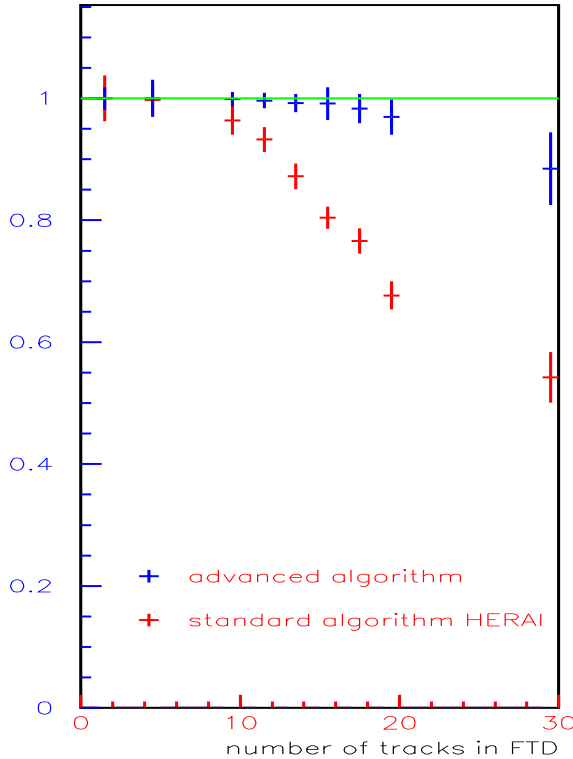
Number of tracks in FTD	Efficiency (simulation)			Efficiency (data)
	Purity 60%	Purity 80%	Purity 95%	
10	98%	95%	90%	100%
20	96%	91%	88%	100%
30	94%	87%	78%	85%

figure 2). The intersection of clusters from different modules define segments. At high multiplicities, e.g. more than 20 tracks, the combinatorics means that intersections of only two clusters have very low purity. Therefore, a segment is defined to be the intersection of three or more clusters. All intersections between any two clusters in a supermodule are found and fitted to a straight line at a fixed  $z$  (the P-module wire closest in  $z$  to the Q modules). In this way, each intersection is represented by a point in  $(X, Y, X', Y')$  space. If a track is perfectly measured and found in all five modules within a supermodule, then there will be ten intersections all within close proximity in the four dimensional space. The existence of three or more lines of intersection is considered a candidate segment, in order to account for detector effects.

Candidate segments are identified as spikes in the four dimensional intersection fit space  $(X, Y, X', Y')$  and are found in a similar way to the cluster spikes described previously. The fit results from all of the two cluster intersections are ordered in each dimension. A scan is made for a gap above a given threshold, which is tuned for each dimension using Monte Carlo and corresponds to several times the detector resolution in that dimension. Candidate segments are three or more intersections within a given intersection spike. For each of the candidate segments, all of the hits belonging to each of its clusters are fitted to a straight line. In order to identify true track segments, these candidate segments are fed into an algorithm which finds a disconnected set using a connectivity table. The algorithm developed for disconnecting the set of connected candidate segments looks for any singly connected segments and removes them. If there is more than one such candidate, the one connected with the highest chi-squared probability is removed first. The connection probability is again defined as in equation 3.1, where now the sum is over the chi-square and degrees of freedom of the connected segments. If no singly connected segments exist then the candidate segment which is connected with the highest connection probability is removed, consistent with it being in the set of segments with the highest number of connections to other segments. The algorithm is repeatedly applied after a candidate segment is removed until a disconnected set remains.

### 3.3.2 Segment forming efficiency

The efficiency for finding segments is shown in figure 7 as a function of the number of tracks in the FTD. The plot shows the segment finding efficiency for tracks which have a purity greater than 60% (the great majority of tracks have a purity of nearly 100%). The red points show the efficiency for the old FTD with the old software algorithms. The blue points show the same for the new



**Figure 7.** Figure showing the efficiency of segment finding in the FTD as a function of track multiplicity, comparing the old detector and software (red) with the new detector and software (blue).

FTD and the new algorithms. A large improvement at high multiplicities is clearly demonstrated with an efficiency of 100% at low multiplicities, remaining around 90% for an event with 30 tracks in the FTD. For context, the number of segment candidates found increases with increasing track density, such that the algorithm for finding the disconnected set of segments is crucial. At twenty tracks,  $\sim 75\%$  of the candidate segments must be accurately removed in order to uncover the true tracks. This is achieved with such accuracy that an efficiency of approximately 97% is obtained. It is clear that the upgraded FTD, together with this pattern recognition is a great improvement on the previous FTD and has good efficiencies for most topologies. The segments from this stage are then passed to a linking stage to make them into tracks, which uses the same algorithm as described previously [1].

## 4. Improvements in the Pattern Recognition using a Kalman Filter

### 4.1 Introduction

Essentially the same Kalman Filter framework as described in [1] is used to determine the optimum track parameters for each track in the FTD, albeit with two major additional modifications (other than those necessary to treat the new Planar chambers rather than the old Radial chambers). These modifications are to add pattern recognised track clusters to a track during the Kalman filtering and then to selectively reject track clusters from a track should it fail to be accepted after the Kalman

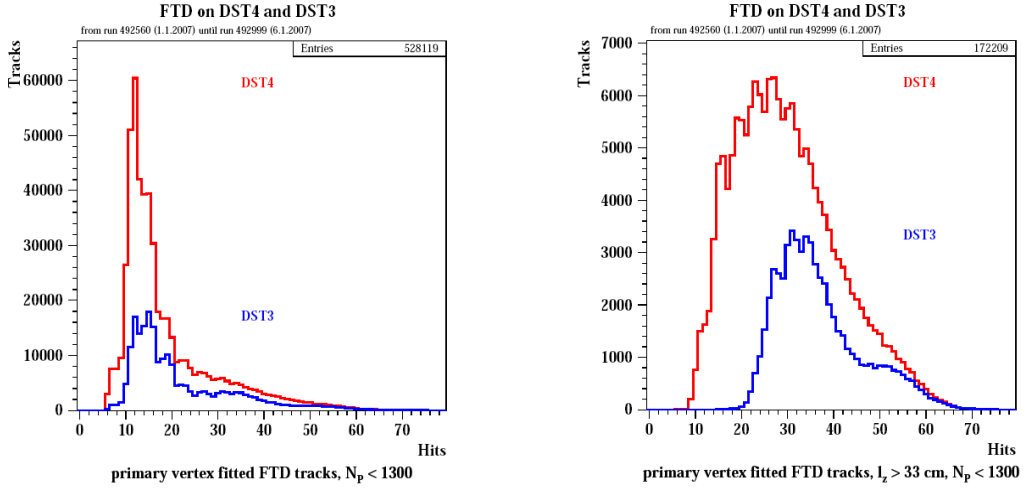


**Figure 8.** The number of hits on tracks found in the original implementation (DST3) and with the cluster addition and rejection modifications (DST4) for all Forward tracks (left) and for Forward tracks passing through more than one supermodule (right).

filter, until the resultant track is acceptable. Both of these are techniques for adding or removing pattern recognised objects to or from the track which is otherwise processed on a point by point basis as the filter moves from measurement surface to measurement surface. The first modification compensates for inefficiencies in the detector or the pattern recognition within a single supermodule such that unused clusters may be attached to a track found in the other supermodules and the second allows pattern recognition mistakes to be removed from a track.

The effect of these modifications is clearly visible in figure 8 which shows the number of hits on tracks found in the original implementation (DST3) and with the cluster addition and rejection modifications (DST4) for all Forward tracks (left plot) and for Forward tracks passing through more than one supermodule (right plot). The structure arising from tracks being found in one, two or all three modules is clearly visible in the original, whereas the in-fill from the first modification and outlier rejection from the second result in the distribution of the number of hits on tracks in the end result being much smoother, suggestive of the resultant tracks being pattern recognised in the FTD as a whole. These two modifications are described separately below.

#### 4.2 Cluster addition

The original implementation of the Kalman Filter in the FTD already included the option to add hits during both the filtering and smoothing steps. Unfortunately the lack of constraint on individual hits meant that this was not particularly useful and the code was never used in production. The modification was to use this existing code, but with a preselection as to which hits may be considered for addition. The Kalman Filter steps from one measurement surface to the next, first from the interaction point outwards (filtering) and then back (smoothing). At the transition between modules or orientations the preselection checks if there are no hits on the track in the module just entered. If so, it then projects the incoming track state vector through each measurement surface in the module and searches to see if there is a nearby unambiguous unused candidate cluster in

this module, respecting the resolved left/right ambiguity in the pattern recognised cluster. If so, at each measurement surface within the module it then uses the existing pointwise code to consider whether to add the point from this cluster, again respecting the resolved left/right ambiguity. If on any pass through the FTD a hit is added the filter then iterates until there has been a complete filter and smooth pass without adding any points. Finally, should the filter fail for any reason during this process the code reverts to the original implementation without attempting to add any clusters.

### 4.3 Cluster rejection

Again, the original implementation of the Kalman Filter in the FTD already included the option to reject hits during both the filtering and smoothing steps. However the covariance matrix proved poorly behaved when removing the contribution from the point being rejected, even when using double precision for all arithmetic. An alternative prescription was therefore adopted. The Kalman filter was run to completion without point rejection. The resultant track quality was then examined and if acceptable no further action taken. If however, the track would then be rejected, it was rather reprocessed, using the final state vector as input but removing the cluster contributing most to the overall errors, iterating until either the resultant refiltered track was acceptable or too few clusters remained on the track.

## 5. Combining FTD and CTD Information

### 5.1 Vertex fitted tracks

The FTD constructs a vertex candidate, with moderate precision, from FTD tracks using a weighted average of the  $z$ -information from each track. A superior vertex is formed from the CTD, which incorporates information from all of the tracking detector technologies in the central region of the H1 detector. This vertex candidate has very high precision, thanks largely to the silicon detectors located close to the H1 beam pipe[3]. Only in the rare cases where the CTD fails to find a vertex candidate is the FTD vertex candidate used. The track-to-vertex fitting process simply adds the vertex as a spacepoint in a Kalman Filter fit of the forward track, yielding improved parameters for that track. The resultant track is referred to herein as a "Forward" track.

### 5.2 Combined FTD and CTD tracks

Linking of tracks reconstructed using the CTD ("Central") and FTD to form "Combined" tracks is performed in order to produce tracks which, in principle, have more precise estimates of the true track parameters (assuming that the correct associations are made). Tracks from each device are extrapolated to the inner surface of the CTD end-wall, with track parameters and their associated measurement errors, including multiple Coulomb scattering contributions using the Kalman Filter. The two sets of track parameters are then compared, potential links identified and ambiguities resolved. The parameters of surviving matched track pairs are combined using a weighted average.

The inputs to the combination algorithm are the lists of Central and Forward tracks. The two track types use two different parameterisations to represent the track, shown in table 2.

These are different due to the orthogonal sense-wire geometries of the two trackers; tracks in an intermediate range of polar angles (between approximately 20 and 70 degrees) can be represented in either form, but in general they are not interchangeable. Note that the  $z$  coordinate in Type

**Table 2.** Track parameterisation types used for Central and Forward tracks.

	Type 1 (Central)	Type 2 (Forward)
Curvature	$1/r$	$1/r$
Azimuthal angle	$\phi$	$\phi$
Polar angle	$\theta$	$\theta$
Position 1	$dca$	$x$
Position 2	$z_0$	$y$
Location	-	$z$

2 is not a fit parameter (i.e. it has no error); it just specifies where on the track the other parameters are given. The equivalent parameter for Type 1 is implicit, as the parameters are always given at the point of closest approach to the  $z$  axis.

Central and Forward tracks are extrapolated to the common  $z$ -plane (the CTD end-wall) using the Type 2 parameterisation. The Forward track parameters are first corrected for any misalignment between the Forward and Central trackers, using pre-determined translation and rotation adjustments (see section 5.3). Multiple scattering is allowed for by increasing the extrapolated covariance matrix, assuming material with known radiation length between planes either side of the CTD end-wall. Energy loss is corrected using a Bethe-Bloch parameterisation and the same approximate model for material, with the assumption that the track is a pion.

A list of (possibly ambiguous) associations between Forward and Central tracks is created by looping over all extrapolated Central tracks, and for each of these calculating a chi-squared with each Forward track, using the extrapolated track parameters. Candidate associations with an acceptable chi-squared are kept. All Forward tracks with only one associated Central track are accepted as a Combined track candidate. Ambiguities are resolved and links chosen by looping over all Forward tracks and choosing the association with the minimum chi-squared<sup>6</sup>. After each link is made, any other associations with the same Central track are deleted, so that the final list of links is unambiguous. Finally, the Combined tracks themselves are created by taking the weighted mean of the two sets of track parameters and are then transformed to the Type 1 parameterisation.

### 5.3 Alignment to the CTD

The residuals measured at the CTD end-wall in the track-linking procedure, in  $x$ ,  $y$ ,  $\theta$  and  $\phi$ , provide important constraints on the relative alignment of the FTD and CTD, they are shown in figure 9. By convention H1 chooses the CTD as its reference system, with respect to which all other sub-detectors must be aligned. Regarding the FTD as a rigid body, there are six degrees of freedom that determine its relative alignment with respect to the CTD; a three-vector translation to align its coordinate origin with that of the CTD, plus three Euler rotations that define the relative angular orientation of the two systems. Thus, the residuals monitored in the track linking provide half of the

---

<sup>6</sup>If there are multiple associations, Central tracks with a larger number of hits are preferred even if they have a larger chi-squared than an association with a track having fewer hits. This means that Central tracks with  $z$ -chamber hits are preferred as such tracks have a superior  $z$ -resolution.

six required alignment constraints (the  $\phi$  residual effectively measures one of the three Euler rotations). The other three constraints can be derived from the track-to-vertex fitting process described previously, with the residuals in  $x$ ,  $y$  and  $z$  with respect to the vertex providing the information. The final set of six alignment parameters (a three-vector translation plus three Euler rotations) are used to align Forward tracks to the rest of H1. The equations relating these six parameters to the six observed residuals are non-linear and are solved numerically, using an iterative procedure to derive the parameter set that minimise (to zero) the observed six alignment residuals.

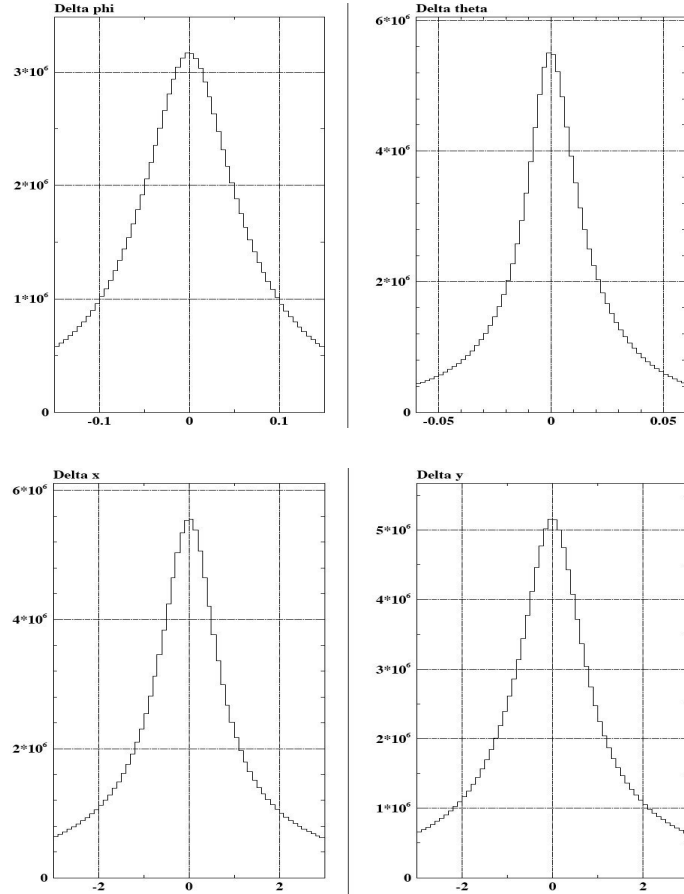


**Figure 9.** (top) Delta phi and Delta theta (radians) and (bottom) Delta x and Delta y (cm) between Forward and Central tracks at the CTD end-wall.

## 6. Performance of the HERA II FTD

The performance of the FTD has been assessed using Monte Carlo simulation and real data. The simulation of the FTD is described in [1]. It should be noted that, for HERA II, the track-related noise simulation and parameterisations of the pulse shape fluctuations are not used. However, the efficiencies of the detector were tuned to match those seen in data. In the following, Forward tracks are studied, with a vertex which is always defined by the CTD. The tracks must pass a selection, detailed in section 6.1, and the resulting FTD performance is monitored using independent H1

detectors. Data is compared to the simulation for both an inclusive sample of deep-inelastic scattering (DIS) events and an elastic  $J/\Psi$  sample of events, representing high and low multiplicities, respectively.

### 6.1 Track selection

The surroundings of the FTD further complicates track reconstruction in an already demanding environment. The readout electronics of the CTD in the CTD end-wall are situated directly between the CTD and the FTD and constitute approximately  $X_0/2$  of dead material. This dominates the multiple scattering component of the FTD resolution and makes low momenta inaccessible. A collimator is situated directly underneath the FTD and generates many extra tracks from secondary interactions with the proton remnant. Therefore, only a portion of the tracks which are reconstructed by the FTD are useful for physics analysis and a selection is applied to Forward and Combined tracks<sup>7</sup>. Tracks passing this selection are used in the HFS algorithm of H1. The selection is given in table 3.

**Table 3.** The cuts used to select Forward (left) and Combined tracks for physics analyses.

Cut motivation	Forward	Combined
Fiducial	$6^\circ < \theta < 25^\circ$ RadialStart $> 25$ cm	$10^\circ < \theta < 30^\circ$ RadialStart $< 50$ cm
Pointing	$R0 < 20$ cm	$DCA' < 5$ cm
FTD-only	NHits $> 10$ $z_e - z_s > 10$ cm	
Reliable measurement	$p > 0.5$ GeV $p_T > 0.001$ GeV	$p > 0.5$ GeV $p_T > 0.12$ GeV
Outlier removal	$dp/p < 9999.9$ $\chi^2(\text{VF}) < 25$ $\chi^2(\text{Track}) < 10$	$dp/p < 9999.9$ $\chi^2(\text{VF}) < 50$ $\chi^2(\text{Link}) < 50$

The selection can be broken down into three components. Fiducial cuts are applied to ensure that the track originated from an  $ep$  collision close to the nominal interaction point. The requirement of a minimum starting radius of a Forward track avoids the areas of the detector most affected by ageing, while the maximum starting radius for Combined tracks ensures good overlap with the CTD. FTD tracks are required to have a minimum length and number of hits to ensure good detector acceptance (Combined tracks have an inherently good acceptance with the additional CTD information). A minimum momentum cut of 0.5 GeV is applied in order to have good acceptance (the particle should have enough energy to get through the CTD end-wall). The minimum transverse momentum cut for Combined tracks is applied to ensure that the central track component is well measured. Finally, tracks with very poor momentum measurements and outliers in the  $\chi^2$  distributions are removed as such tracks are not well simulated.

<sup>7</sup>Studies of track parameters and their errors showed that the track selection also improved the scaled residuals for track parameters.

## 6.2 Comparisons of data and simulation for inclusive NC events

Inclusive DIS events at high  $Q^2$  and  $x$  produce large numbers of particles in the forward region from the struck parton. In principle, the kinematics of neutral current DIS events can be reconstructed solely from the kinematics of the scattered electron, but an improved resolution is achieved if the kinematics of the hadronic final state (HFS) are also included. In the case of charged current DIS events, the kinematics must be measured from the HFS alone. In the following, a standard inclusive neutral current DIS selection is used to select a sample of events which are globally very well described by simulation.

Forward and Combined tracks which pass the track selection in section 6.1 are studied using tracks reconstructed by the FST and CTD detectors. Track quality selections are applied to tracks from the FST and CTD and in addition the tracks are required to have  $p > 0.5$  GeV. A Forward (Combined) track is matched to an FST (Central) track if  $|\Delta\theta| < 0.03$  mrad and  $|\Delta\phi| < 0.1$  mrad. Figure 10 shows the efficiency of Forward and Combined tracks as measured by the FST and CTD, respectively. The efficiency is studied as a function of  $\theta$ ,  $\phi$ ,  $p_T$  and track multiplicity in the FTD. All efficiencies are described to within 10% or better by the simulation. The value of the efficiency is low compared to the single-track reconstruction efficiency of the FTD, which approaches 100% with the same selection applied (see section 6.3). This can be understood as being a consequence of the high density environment and is well described by the simulation. The number of clusters and segments used in the Forward and Combined tracks is shown in figure 11. It is very well described by the simulation and the effect of the CTD acceptance can be clearly seen in the case of Combined tracks.

The track parameters of Forward and Combined tracks are studied using the CTD, which has a superior resolution to the FTD. Figure 12 shows the difference in  $\theta$ ,  $\phi$  and  $p$  for matched tracks. Both  $\phi$  and  $p$  are in good agreement with the CTD and this is well described by the simulation, while  $\theta$  shows a bias which is slightly larger than that in the simulation. Studies using the FST show the same features but the resolution is dominated by the resolution of the FST. As  $\theta$  is the least well constrained parameter in the alignment procedure, due to the FTD's poor  $z$  resolution and the highly non-linear relation between  $z$  residuals and a  $\theta$  alignment, this is understood.

Finally, the momentum measurement and the error on the momentum measurement as a function of momentum are shown in figure 13 for both Forward and Combined tracks. Both track types are described very well by the simulation with Combined tracks having approximately a factor two better resolution, as expected.

## 6.3 Comparisons of data and simulation for elastic $J/\Psi$ events

The hostile environment of the forward region of H1 in inclusive DIS events, where there is typically a lot of activity, makes it difficult to cleanly define a single-track efficiency in data. The elastic  $J/\Psi$  process, where the proton escapes elastically down the forward beam pipe, alleviates this problem. Furthermore, the di-muon decay channel provides a clean experimental signature with minimum influence from the abundant dead material situated in front of the FTD. The Forward Muon Detector (FMD) and Forward Iron Endcap (FIE) provide independent measurements of the forward-going muon at low angles, supplementing the CTD.

**Table 4.** Reconstructed mass of  $J/\Psi$  candidates in GeV using a Control, Combined or Forward track for the forward muon.

	Data	Simulation
Control	3.08	3.09
Combined	3.06	3.06
Forward	3.07	3.06

In the following,  $J/\Psi$  candidates are selected with one forward muon ( $\theta < 30^\circ$ ) and one central muon ( $\theta > 30^\circ$ ), using the standard H1 muon reconstruction. The elastic nature of the event is guaranteed by there being no energy deposit in the H1 calorimeter above 500 MeV, other than energy associated with either of the muons. Events are only kept if the two muon tracks are of opposite charge. The forward muon must have a signal in the FMD or FIE detectors. The CTD is most often used to reconstruct the kinematics of the forward muon but if the CTD fails to do that then these auxiliary detectors are used instead. The muon thus reconstructed is referred to as the "Control" muon. This allows the efficiency of the FTD to be determined in a very clean environment but despite this, the track selection given in section 6.1 is applied to Forward and Combined tracks. If a selected Forward or Combined track is found, it is used together with the central muon to reconstruct a  $J/\Psi$  candidate, allowing the momentum scale of the FTD to be studied.

The di-muon mass spectrum using Combined and Forward tracks to reconstruct the forward muon can be seen in figure 14. Both data and simulation are in reasonable agreement with the PDG value for the  $J/\Psi$  mass of 3.095 GeV and a clear  $\Psi'$  signal can also be seen. Table 4 shows the fitted mass values using a Breit-Wigner function for different track combinations. The 0.5% underestimate for the control sample compares reasonably well with the 1% underestimate in the case of using a Combined or Forward track. The underestimate is well reproduced by the simulation and is attributed to the lack of detailed description of the CTD end-wall which is used to calculate the energy-loss correction. The width of the invariant mass spectrum is also well described by simulation.

Figure 14 also shows the efficiency for finding either a Forward or a Combined track. The efficiency of the FTD is close to 100% at best in data, while the simulation tuning applied to describe inclusive DIS data results in a significant underestimate in the simulation. At large  $\theta$  the efficiency is shaped by the detector acceptance, while for  $\theta < 10^\circ$  the efficiency downturn is entirely the result of the track selection. If the tuning is not applied to the simulation, the efficiency is very well described.

## 7. Summary

The upgraded Forward Track Detector of H1 for the HERA II phase has been presented. The detector hardware was significantly modified in order to improve the detector performance. Upon commissioning the detector, ageing was found to have affected the old Planar chambers that were still in use. A new QT algorithm was developed to allow the chambers to be operated at lower gain

and mitigate the effects of ageing, which successfully restored the single hit efficiency to  $\sim 96\%$ , allowing the chambers to be operated at close to design parameters for the rest of HERA running, with an uptime of  $\sim 98\%$ .

The software of the FTD was rewritten to take advantage of the improved hardware. The performance of the new algorithms using the new hardware configuration surpassed the previous incarnation of the FTD, with very high cluster and segment finding efficiencies achieved together with high purity. The Kalman filter used to produce the final tracks from the reconstruction was modified to further improve the track reconstruction, adding and rejecting clusters to improve the overall track quality of Forward tracks. These Forward tracks were combined with central tracking information to provide Combined tracks with improved precision, while providing a framework to align the FTD to the rest of H1.

The performance of the FTD was measured using several independent detectors, chiefly the CTD. In inclusive NC DIS events, the description of Forward and Combined tracks, after a track selection, by the H1 simulation (tuned to match the observed cluster-finding efficiency in data) is good. While the efficiency of the FTD for reconstructing Forward and Combined tracks is relatively low ( $\sim 30 - 50\%$ ) in this high multiplicity environment, it is well described by the simulation, also differentially. The track parameters of selected Forward and Combined tracks are accurate and are again well described by simulation, allowing these tracks to be used in the H1 HFS algorithm. Finally, using a sample of elastic  $J/\Psi$  events, the FTD was shown to have an accurate and well simulated momentum measurement and a single-track efficiency of close to 100%.

## References

- [1] S. Burke, R. C. W. Henderson, S. J. Maxfield, J. V. Morris, G. D. Patel, D. P. C. Sankey and I. O. Skillicorn, *Nucl. Instrum. Meth. A* **373** (1996) 227.
- [2] I. Abt *et al.* [H1 Collaboration], *Nucl. Instrum. Meth. A* **386** (1997) 310;  
I. Abt *et al.* [H1 Collaboration], *Nucl. Instrum. Meth. A* **386** (1997) 348;  
R. Appuhn *et al.* [H1 SPACAL Group], *Nucl. Instrum. Meth. A* **386** (1997) 397.
- [3] D. Pitzl, O. Behnke, M. Biddulph, K. Bosiger, R. Eichler, W. Erdmann, K. Gabathuler and J. Gassner *et al.*, *Nucl. Instrum. Meth. A* **454** (2000) 334 [[hep-ex/0002044](#)].  
B. List, *Nucl. Instrum. Meth. A* **501** (2001) 49.

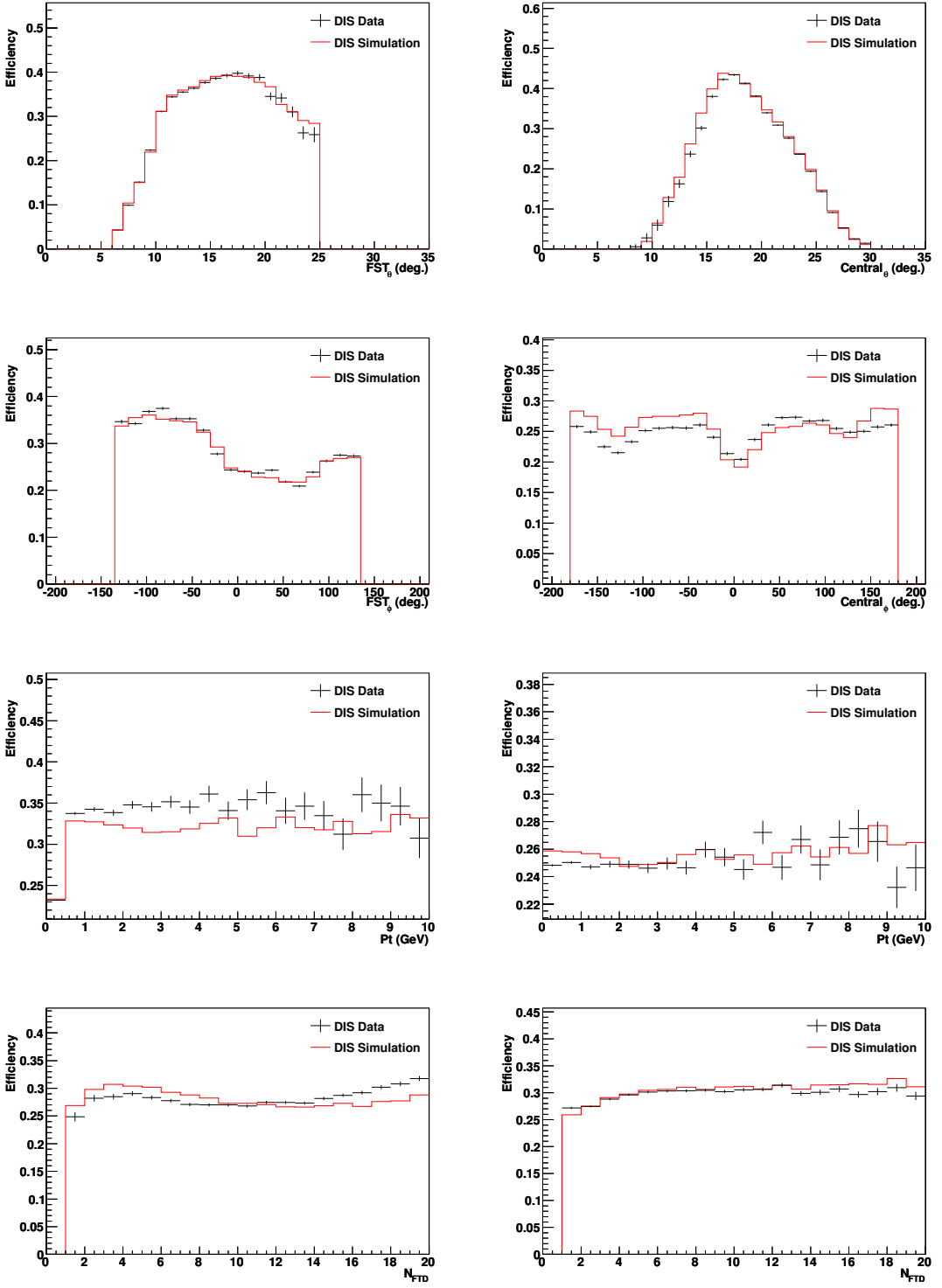


**Figure 10.** The efficiency of finding a matched Forward (Combined) track as measured by the FST (CTD) as a function of  $\theta$ ,  $\phi$ ,  $p_T$  and FTD track multiplicity. Forward tracks are studied in the left column, Combined tracks in the right.

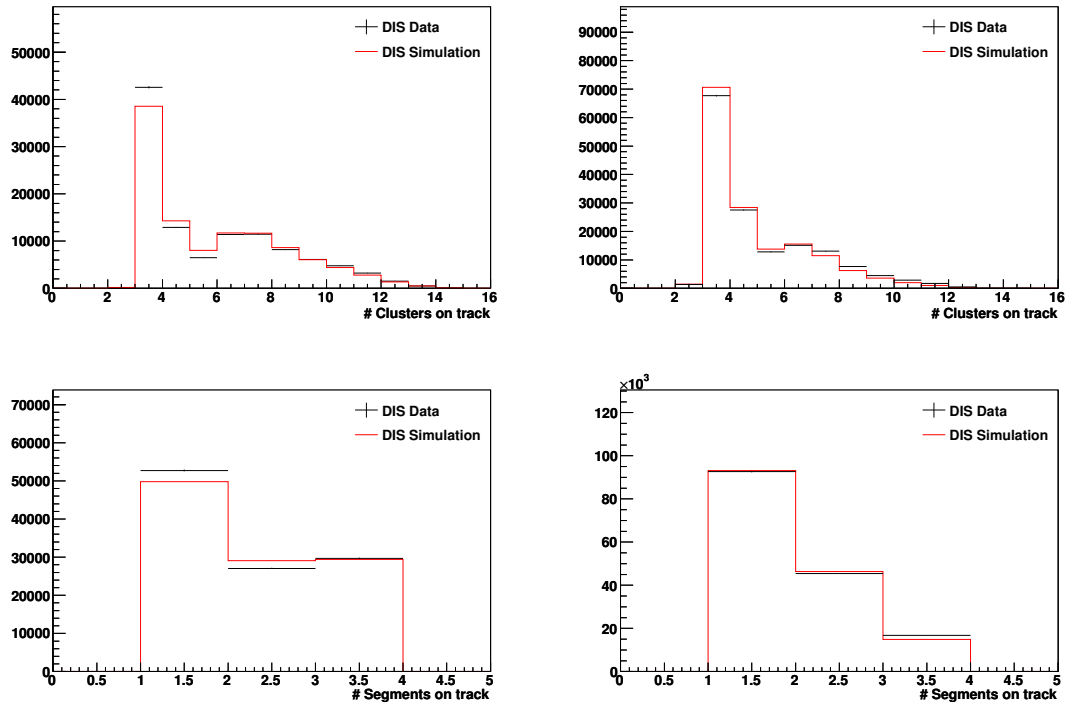


**Figure 11.** The numbers of clusters and segments on Forward (Combined) tracks, shown in the left (right) column.

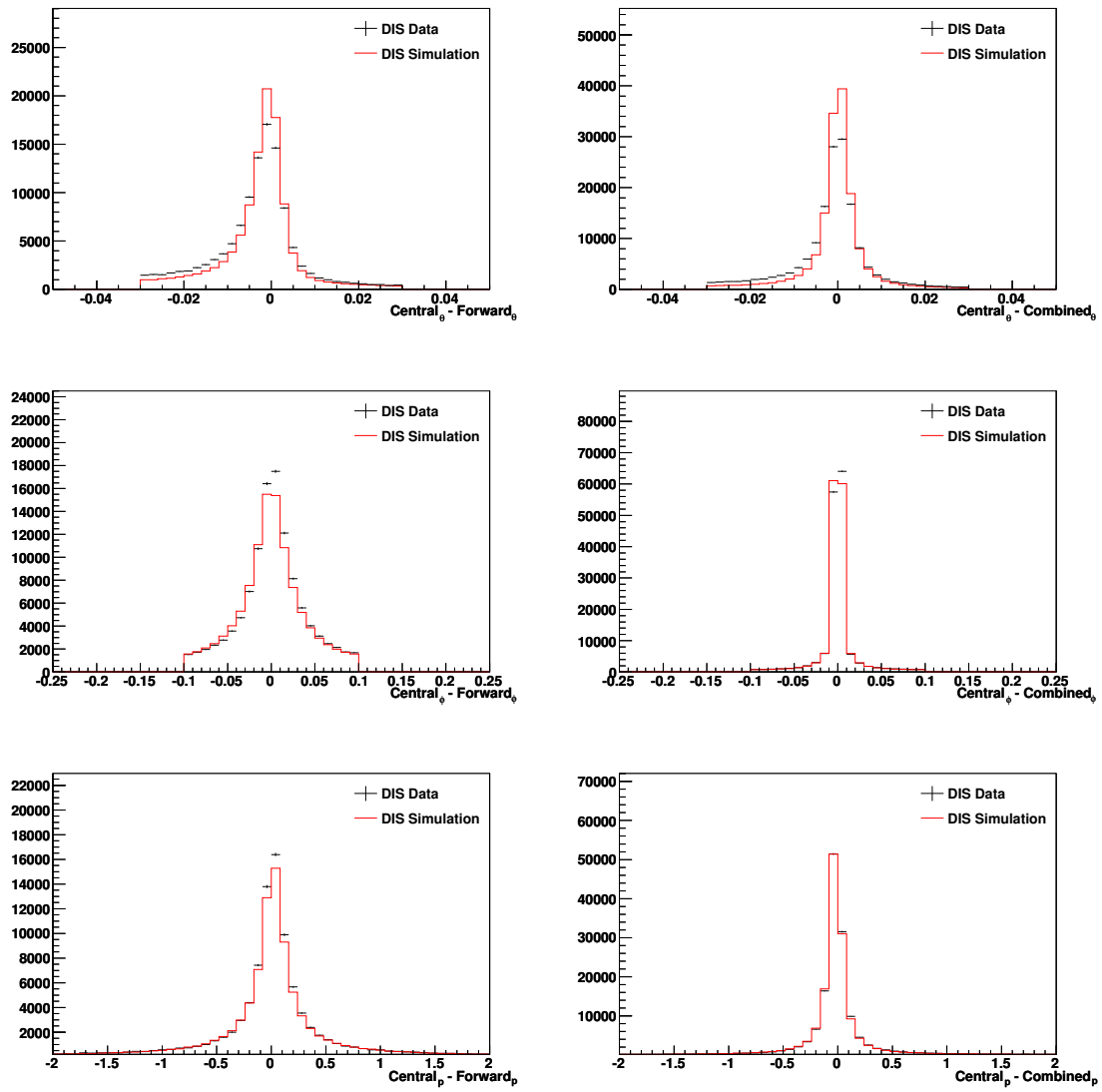


**Figure 12.** The difference in  $\theta$ ,  $\phi$  and  $p$  for Forward (Combined) tracks matched to Central tracks in the left (right) column.

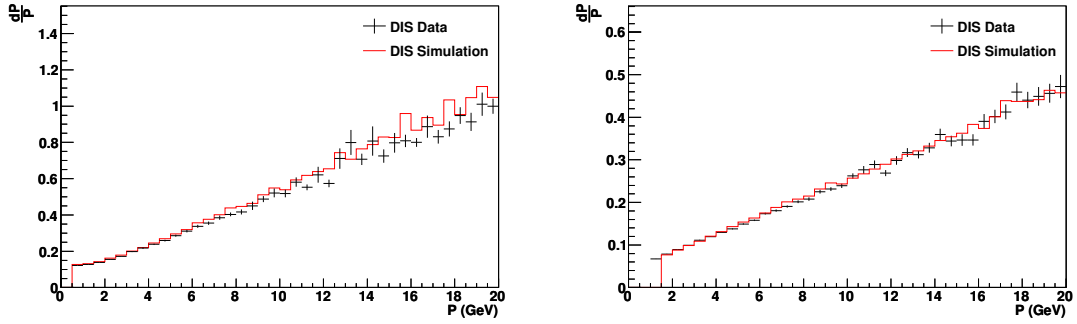


**Figure 13.** The significance of the momentum measurement  $dP/p$  as a function of  $p$  for Forward (left) and Combined tracks.

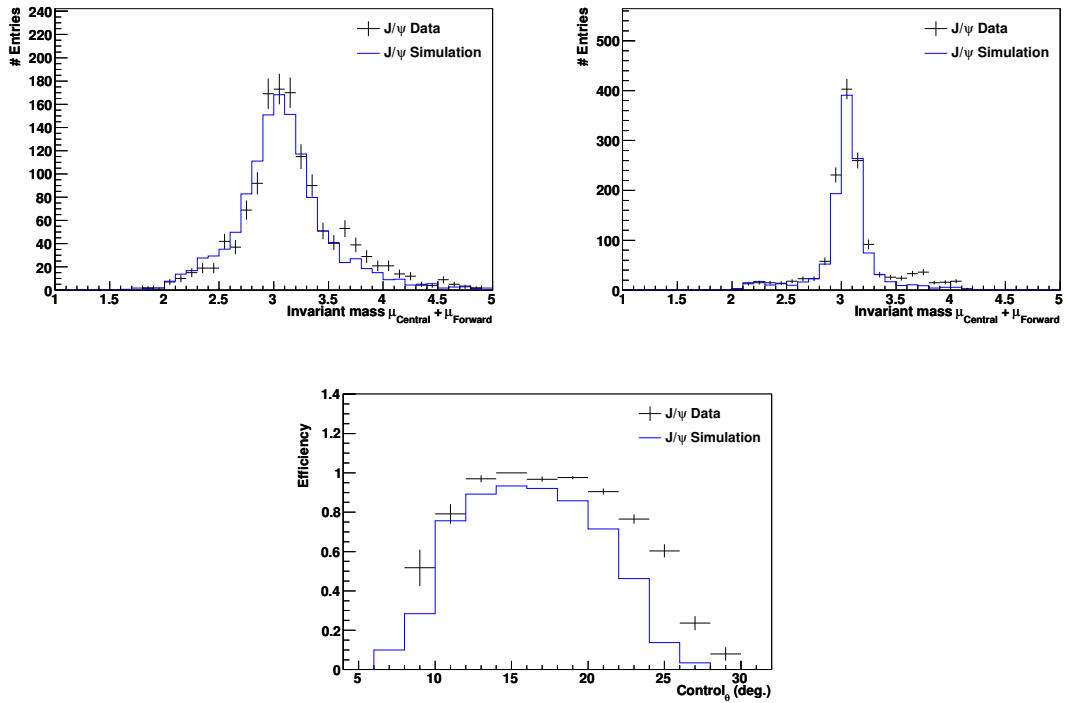


**Figure 14.** Invariant mass of  $J/\Psi$  candidates reconstructed using a Forward (left) or Combined (right) track for the forward muon measurement, and (bottom) the efficiency of finding either a Forward or a Combined track.